762 *KSME International Journal, Vol. 13, No. 10, pp. 762~774, 1999*

Direct Simulation of Effective Conductivity of Porous Silicon: Fourier Treatments

Jae Dong Chung*

(*Received January 20, 1999*)

The effective thermal conductivity of anisotropic porous-silicon layers is predicted using the simulated pore structure from a two-dimensional, diffusion-limited model along with the Fourier conduction. The low-dimensionality effect due to the phonon boundary scattering is included through an available modified solid conductivity, It is shown that for the highly branched columnar structure, the effective conductivity across the layer is small and yet much larger than that along the layer. Good agreement is found with available experimental results. It is predicted that the combination of a small pore size and a high porosity leads to a very small effective conductivity. This makes porous-silicon layer an attractive insulator and readily integrable in silicon-based microstructures. In a following paper, the low-dimensionality effect is directly included in a Boltzmann treatment of phonon transport.

Key Words: Effective Conductivity, Porous Silicon, Fourier Treatment, Size Effect.

Nomenclature

ρc : Volumetric heat capacity (J/m³K)
d : Pore size (m)
k : Thermal conductivity (W/m-K)
$\mathbf{K}$: Thermal conductivity tensor (W/m-K)
L : Length (m)
q : Heat flux (W/m²)
T : Temperature (K)
u : Phonon velocity (m/s)
x : Coordinate along the porous silicon layer (m)
y : Coordinate across the porous silicon layer (m)

Greek

ε : Porosity
λ_p : Phonon mean-free path (m)

Subscripts

f : Fluid
p : Phonon
s : solid
δ : $y=\delta$ location
$\parallel$: Longitudinal
$\perp$: Transverse
0 : $y=0$ location

Other symbols

$\langle\rangle$: Volume averaged value

* Turbo and Power Machinery Research Center Seoul National University Seoul, Korea, Present address: Center for Nano Particle Control, Institute of Advanced Machinery and Design, Seoul National University, Seoul, 151-742, Korea.

1. Introduction

Porous silicon layers are formed on the surface of locally or wholly doped silicon wafers. It can also be formed away from the wafer surface by proper, distributed doping. The etching is by anodic dissolution (i. e., electrochemical etching) of the monocrystalline, impurity-doped silicon in aqueous, hydrofluoric acid (HF) solutions. The porous-silicon layer is depicted in Fig. 1. Due to the pore morphology, the effective conductivity is not isotropic and a preferential conduction heat flow occurs along the y direction. The porous -layer thickness δ may be as small as a few micron and as large as desired (i. e., up to a few

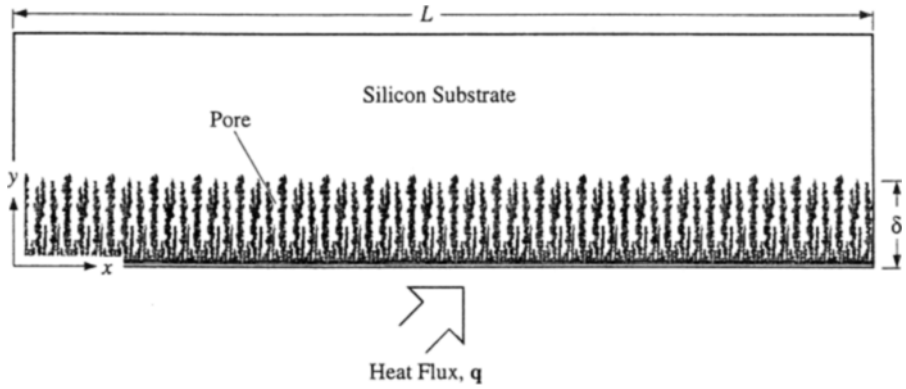

Fig. 1 A schematic of the porous silicon layer considered.

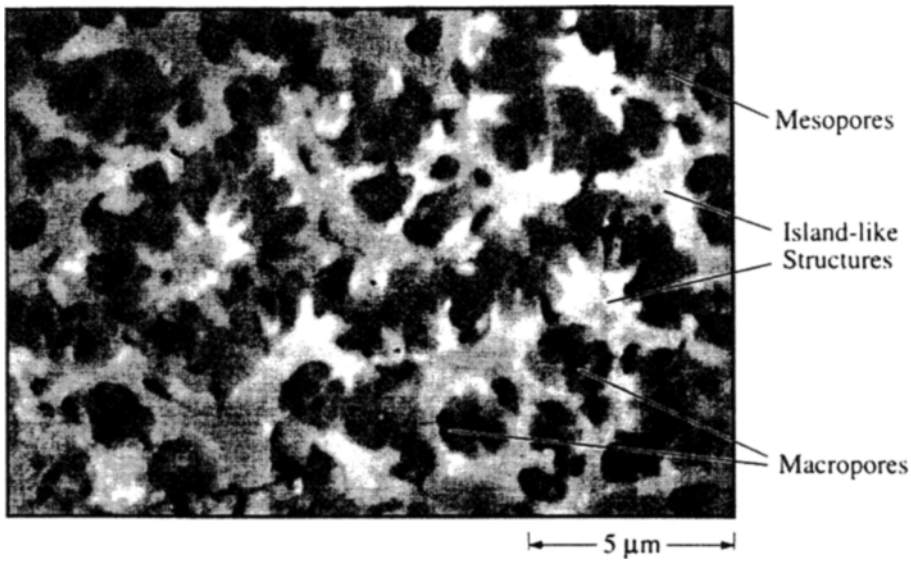

Fig. 2 SEM (top view) of the porous layer etched in a p^- silicon wafer.

hundred micron). Micrograph of a typical porous silicon surface is shown in Fig. 2. Due to its photoluminescence capability and having physical properties greatly different from the bulk material (such as permeability, low effective thermal conductivity, and low density), porous silicon is a promising material in silicon-based integrated circuits and devices. As an example, many thermal sensors operate based on the measurement of a small amount of thermal energy. This minute amount of energy must cause a relatively large temperature change in the sensing medium. This medium must then be small and well isolated from its surroundings and a porous-silicon layer can be used. Although complete backside etching is also possible for insulation, it has a mechanical vulnerability disadvantage compared to the porous-silicon layer. Other applications, and the current knowledge about porous silicon, are reviewed by Canham (1997).

The Fourier treatment of the effective conductivity tensor $\langle \mathbf{K} \rangle$, is made by averaging the energy equation over an elementary volume representing the porous medium. When the porous medium has a periodic structure, successful predictions can be made (Nozad et al., 1985). Recent analytical solutions for periodic structures include that of Bauer (1993) for isotropic-periodic, and Lee

and Yang (1998) for anisotropic-periodic structures. As evident in Fig. 1, porous silicon shows a strong anisotropy, and it is also expected that simple, unit-cell based representations will not be realistic and effective. Kaviany (1995) provides a review along with a number of correlations for the effective conductivity and their conditions of applicability.

In direct simulation of the effective conductivity tensor rather than imposing a prescribed, simple structure, the pore structure can be scanned from micrographs (two- and three-dimensional structures). This has been done by Nishioka et al. (1996) for porous iron (sintered iron particles). The two-dimensional computational grid consists of the same number of pixels as the scanned image. Bakker (1997) also discusses the importance of the including the actual morphology. The low effective thermal conductivity of porous silicon is expected to be due to the low-dimensionality of the pore walls, the tortuous solid conduction path, and the presence of low conductivity of gas (i. e., air) in the pores. However, quantitative analysis of the effective thermal conductivity of porous silicon including the pore morphology, is not available.

Other than the pore morphology, the size effect and the chemical changes (such as oxidization) also influence $\langle k \rangle$. It is expected that the pore-level length scale of porous silicon is small enough so that the phonon boundary scattering in the solid becomes important and resistant to the thermal transport. This causes the phonon (dominant heat carrier in silicon) mean-free path to be terminated by boundary scattering at the surface (Ziman, 1960). This introduces an additional resistance to the heat flow and $\langle k \rangle$ decreases directly proportional to the ratio of the average pore size $\langle d \rangle$ to the bulk mean-free path.

The Fourrier conduction is used to numerically predict $\langle k \rangle$ of porous silicon. The existing pore-network is used from diffusion-limited simulations (Smith and Collins, 1989), which are anisotropic and non-uniform, to allow for the

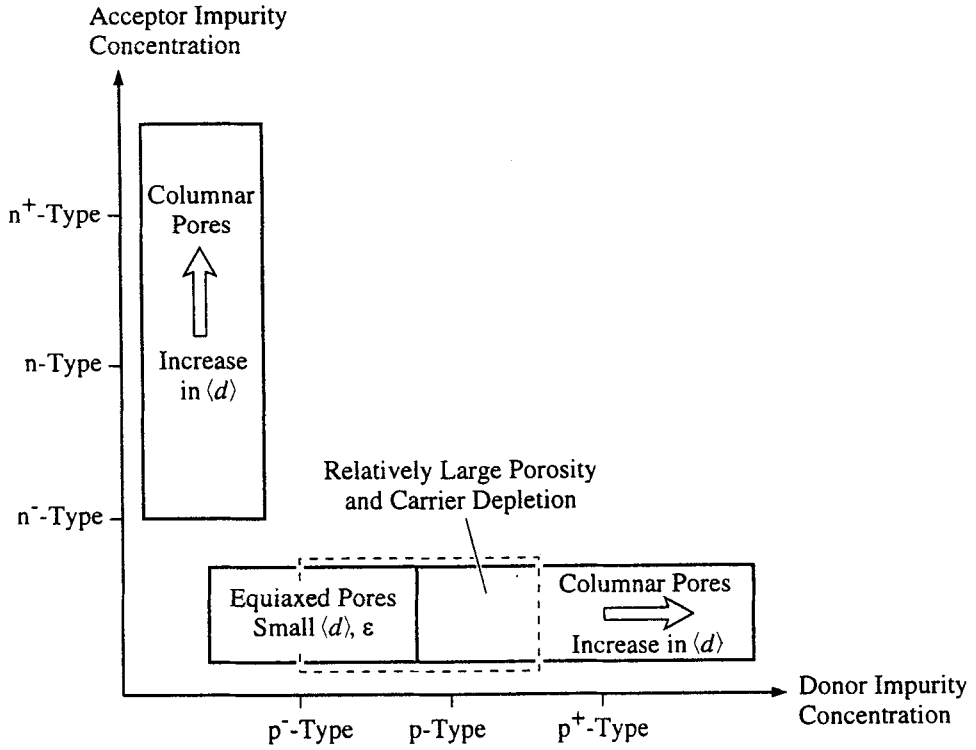

Fig. 3 A classification of the pore morphology, average porosity $\langle \varepsilon \rangle$, and average pore size $\langle d \rangle$ for a n- and p-type porous silicon.

effects of the pore randomness. The available simulations are for lower porosities compared to the available experimental results, and therefore, these simululations are extended to higher porosities using a simple manipulation. The low-dimensionality effect is adressed in this paper. Finally, the predictions are compared with the available experiments.

2. Pore Morphology

The morphology of porous-silicon layers is designated by the average porosity $\langle \varepsilon \rangle$, the average pore size $\langle d \rangle$, the pore-size distribution, and the pore geometry. A wide variety of morphologies is achievable depending on the surface crystal plane orientation, impurity type, electrical resistivity of the doped silicon, and also the electrochemical parameters such as HF concentration, electrical current density, anodization time, front- and back-side irradiation, and temperature. The pore size can be controlled over three orders of magnitude from nanometers to micrometers and the average porosity of the obtained layer $\langle \varepsilon \rangle$ can be tuned from 0.1 to 0.9.

The pore morphology is characterized by the presence of mesopore and macropore structures. The geometry of the mesopore structures can be divided into columnar (i. e., anisotropic) and equiaxed (i. e., isotropic) structures. For the p^--type silicon wafers, $\langle d \rangle$ is generally small and the structure is equiaxed. For the p^+-type, $\langle d \rangle$ is larger and the pores are more columnar. The trend is basically the same for the n-type silicon (Tsao et al., 1991; Beale et al., 1985). The n-type silicon etched with a light illumination is very similar in structure to the p-type silicon. However, the pore diameters in n-type silicon (100 nm or more) are considerably larger than the p-type silicon. An overview of the different morphologies is given in Smith and Collins (1992). Figure 3 presents a summary of the above morphological characteristics of the porous silicon layers with the impurity as a variable.

The mechanisms of porous silicon formation has been extensively studied but is not completely clear. The diffusion-limited model, proposed by Smith et al. (1988), is one of the accepted models

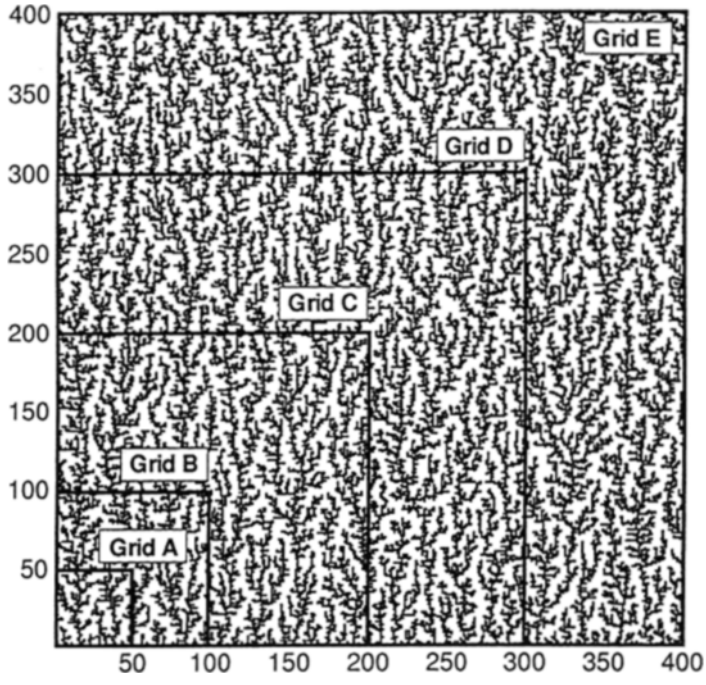

Fig. 4 The pore network and grid system used. Here the average porosities $\langle \varepsilon \rangle = 0.278$ obtained from diffusion-limited simulations by Smith and Collins (1989)

for the pore formation. It explains the pore formation from the diffusion of an electroactive species, such as holes and electrons, to or from the silicon interface. The computer simulations of the porous silicon formation using the diffusion-limited model, show a striking resemblance to the micrographs. Figure 4 is a typical pore structure obtained from the diffusion-limited simulation. This figure also shows the representative elementary volumes chosen. Each axis gives the grid number in that direction.

For various applications, the porous silicon with high porosity is more desirable, and most experiments have been conducted for this range. However, the simulations by Smith and Collins (1989) are for relatively low porosities. In comparison to the experiments, the low porosity simulations are extrapolated to higher porosities.

In addition to the simple extrapolation, pore structures with higher porosities are generated by using a network model (Hoefner and Fogler, 1988) which allows for pore-level non-uniformities. As the Damköhler number (defined as the ratio of the net rate of dissolution by acid to the rate of convective transport of acid) is reduced, the flow channels become highly branched. This results in a pore structure with high porosity. However, it is difficult to directly apply this structure to the numerical calculation of thermal conductivity due to the different roles of pores in heat and fluid flow. In the worm-hole structure generated by the network model, pores function as a flow path but in porous silicon, they function as a block to heat flow. Resolution is another reason why the structure generated by the network model is not appropriate to the present study. Due to the computer limitation, the nodes used in network model were 30×50. The nature of the network model and 6-coordination number seems to successfully anticipate the qualitative pattern of pore structure, but its resolution is not high enough to study the highly irregular porous silicon structure.

3. Analysis

On a macroscopic scale, conductive heat transfer can be accurately represented by the Fourier law and energy equation as

$$\mathbf{q}=-k\nabla T,\ \nabla\cdot\mathbf{q}=0 \tag{1}$$

From the kinetic theory, the thermal conductivity of non-metallic solids can be related to their other physical properties as (Ziman, 1960)

$$k=\rho c_p u_p \lambda_p/3, \tag{2}$$

where ρc_p is the lattice heat capacity, u_p is the phonon speed, and λ_p is the phonon mean-free path. Noted that there is little attention to the effect of pore randomness on the reduction of heat transfer rate. Also note that there exist regimes of size where laws of macroscopic heat transport are no longer applicable (Majumdar, 1993; Tien and Chen, 1994; Chen, 1998).

Schematic diagrams of the two-dimensional unit cell and random network models of porous silicon are shown in Figs. 5(a) and (b). The room-temperature thermal conductivity of pure silicon ($k_s=149$ W/m-K) is used. The doping effect, which can be significant at low temperatures (Touloukian et al., 1970), is not included. The average pore size $\langle d\rangle$, the average porosity $\langle\varepsilon\rangle$, and the pore morphology are assumed to be independent of depth δ in order to compare the effective thermal conductivity of various porous silicon layers (Beale et al., 1985). Experiments (Gesele et al., 1997) show that the layer thickness does not influence the effective thermal conductivity $\langle k\rangle_{yy}$.

3.1 Solution method and verification

Figure 4 depicts a typical simulated two-dimensional pore structure for porous silicon. The air-filled pores are shaded. The pore structure, which is available as digital data, is used for the grid net. The energy equation, Eq. (1) is discretized using the finite-volume formulation (Patankar, 1980) and then solved using the BASIS solver (Kim and Ro, 1995).

When heat flows across the porous silicon layer, the left and the right control surfaces are taken as adiabatic. The lower and the upper surfaces have prescribed temperatures T_0 and T_δ, respectively. The thermal conductivity jump across the air-silicon interface is presented by the

harmonic mean of k_f (air, k_f=0.0267 W/m-K) and k_s (silicon, k_s=149 W/m-K) (Patankar, 1980).

The effective thermal conductivity tensor $\langle \mathbf{K} \rangle$ and its component across the porous silicon layer $\langle k \rangle_{yy}$, are determined from

$$\langle \mathbf{q} \rangle = -\langle \mathbf{K} \rangle \cdot \nabla T, \ \langle k \rangle_{yy} = -\frac{\langle q \rangle_{yy}}{(T_0 - T_\delta)/\delta}, \quad (3)$$

where the y-direction heat flux $\langle q \rangle_{yy}$ is found from

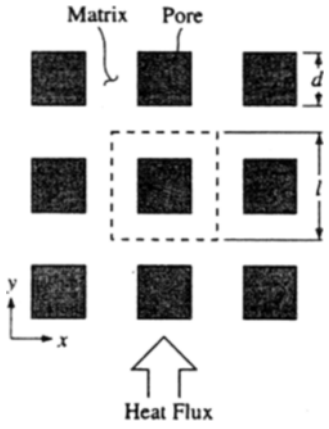

(a) Unit-Cell Model

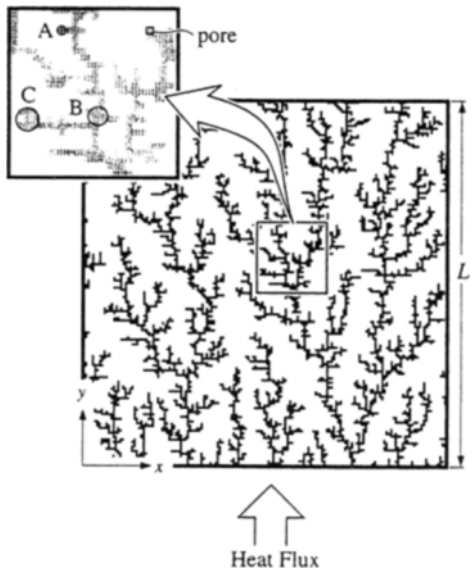

(b) Random Network Model

Fig. 5 Schematic diagrams for (a) the two dimensional unit cell, and (b) the simulated pore-network structure.

$$\langle q \rangle_{yy} = \frac{1}{2L}\left(\int_0^L -k\frac{\partial T}{\partial y}|_{y=0} dx + \int_0^L -k\frac{\partial T}{\partial y}|_{y=\delta} dx \right). \quad (4)$$

The convergence criterion is that the heat fluxes

Table 1 Grid dependency on the average porosity $\langle \varepsilon \rangle$ and the effective thermal conductivity $\langle k \rangle_{yy}$. The asymptotic average porosity is $\langle \varepsilon \rangle_{N\to\infty}$=0.278.

Grid ($M_x \times M_y$)	$\langle \varepsilon \rangle$	$\langle k \rangle_{yy}$, W/m-K
50×50 (A)	0.262	28.27
100×100 (B)	0.277	18.01
200×200 (C)	0.279	17.83
300×300 (D)	0.277	16.31
400×400 (E)	0.277	16.21

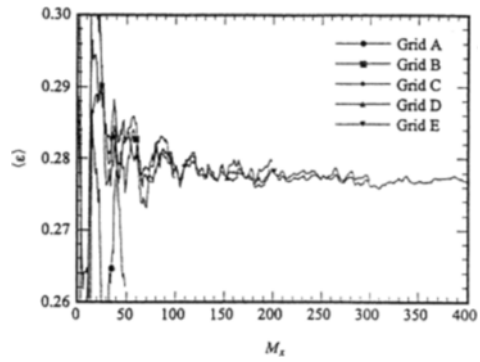

(a) x direction

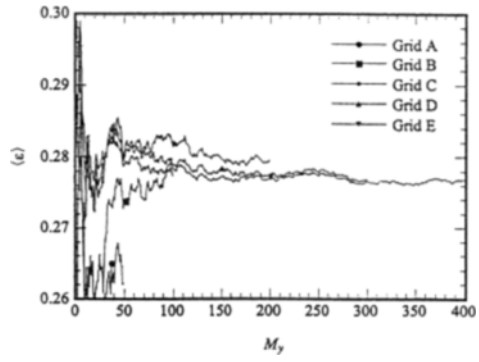

(b) y direction

Fig. 6 The variation of average porosity $\langle \varepsilon \rangle$ along the (a) x direction, and (b) y direction and their dependence on the grid system of Table 1.

at $y=0$ and $y=\delta$ are different by less than 0.01%. The lateral effective thermal conductivity $\langle k\rangle_{xx}$ is found similarly.

Validations were made by comparing the computed $\langle k\rangle$ for a cubic array of square inclusions with those reported in Schneider (1985). Complete agreement was found.

3.2 Selection of representative elementary volume

The representative elementary volume was selected by progressively increasing the grid net until the computed volume-averaged porosity $\langle\varepsilon\rangle$ and effective conductivity $\langle k\rangle$ are no longer change noticeably. Table 1 and Fig. 6 show the grid size effect on the effective thermal conductivity and the average porosity for the asymptotic average porosity $\langle\varepsilon\rangle=0.278$. The corresponding grid nets are shown in Fig. 4, for grid nets A through E. As a compromise, the 300×300 grid (grid net D) is chosen for this microstructure. Note that the meaning of the grid test in this work is different from that of usual numerical approaches. The latter is for reducing the discretization errors but the former is for reducing the locality stemming from the highly non-uniform pore structure. This is why the present grid test shows rough convergence.

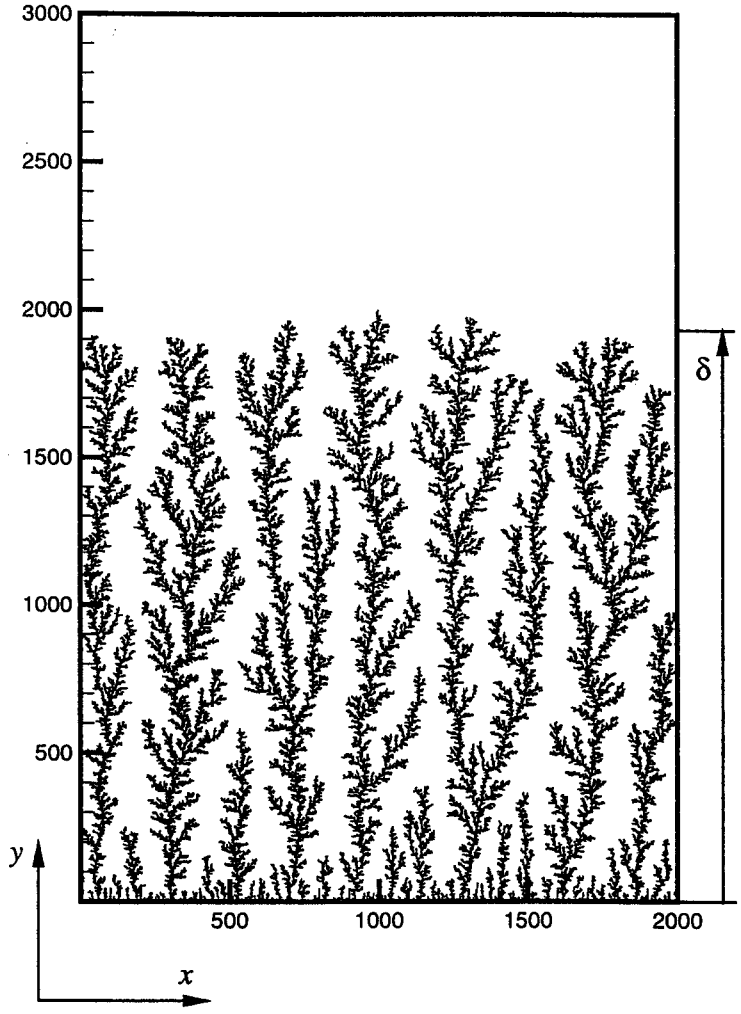

Fig. 7 Typical pore morphology ($\langle\varepsilon\rangle=0.092$) obtained from the diffusion-limited simulation by Smith and Collins (1989).

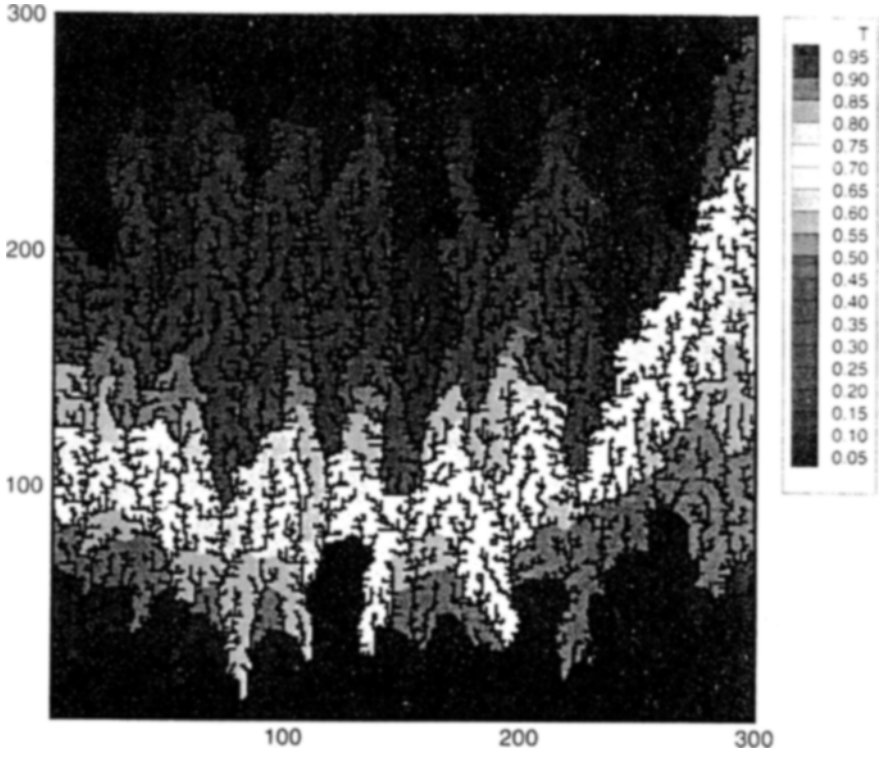

Fig. 8 The pore-network structure and predicted temperature distribution for grid D in Figure 4. The heat flows across the porous layer.

For lower porosities, a larger grid net is needed to reach the asymptotic average porosity and effective conductivity. For example, for $\langle\varepsilon\rangle=0.092$ the computed $\langle k\rangle_{yy}$ may not reach the asymptotic value even when the largest available grid (i. e., 2000×2000) is used. This structure is shown in Fig. 7. Also, note that for columnar structures, the structural (and consequently the transport) anisotropy is quite substantial.

4. Results and Discussion

4.1 Effect of pore-network randomness

To demonstrate the effect of pore-network randomness, $\langle k\rangle_{yy}$ is determined based on the Fourier treatment using the simulated pore-network model. The pore structure and the distribution of the normalized temperature $(T-T_s)/(T_0-T_s)$, for grid D in Fig. 4, are shown together in Fig. 8. The air-filled pores are shaded. Figure 8 shows the high conductivity of solid fingering heat into the layer, while the low conductivity of the air causes a large temperature drop. The isothermal lines follow the high-conductivity solid-phase distribution. Also, note that the random pore structure requires a large representative elementary volume for achieving an asymptotic (grid-size independent) behavior.

For various applications, high porosity (e. g., $\langle\varepsilon\rangle>0.4$) porous silicon is more desirable and most experiments have been conducted for this range. However, the simulations of Smith and Collins (1989) are for relatively low porosities (i. e., $\langle\varepsilon\rangle<0.28$). For comparison with the experiments, the low-porosity simulations can be slightly extrapolated. Two additional pore networks with slightly larger porosities ($\langle\varepsilon\rangle=0.322$ and $\langle\varepsilon\rangle=0.380$) are formed using the available network for the largest porosity ($\langle\varepsilon\rangle=0.278$). Different enlargement factors are applied to the solid

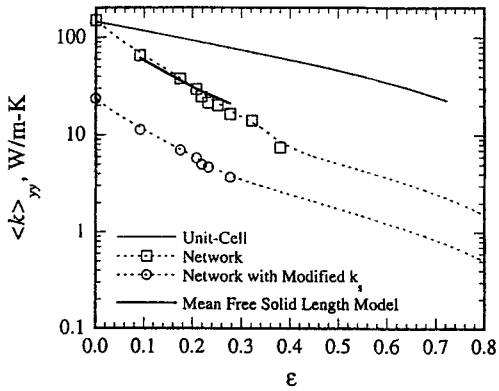

Fig. 9 The effect of pore-network randomness on effective conductivity.

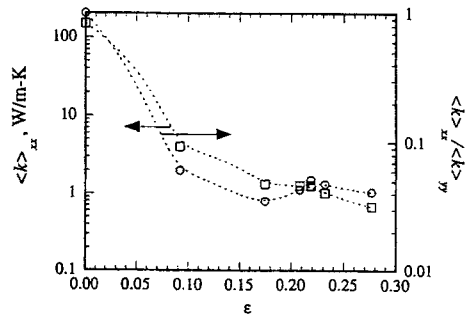

Fig. 10 The predicted variation of the lateral effective thermal conductivity $\langle k\rangle_{xx}$ with respect to porosity ε.

phase and the pore volume. The enlarged domain size is then scaled to its initial value. For validation of this process, a pore network with $\langle\varepsilon\rangle=0.252$, is produced using the available pore network with $\langle\varepsilon\rangle=0.208$. The predicted effective thermal conductivities are found to be in good agreement.

The uncertainty associated with extensive extrapolations is partly due to the highly irregular pore structure and poor availability of a large set of simulated networks. More studies will be needed on the pore formation mechanism and its generation algorithm. The network model will be one of the possible candidates.

Figure 9 shows the predicted variation of the effective thermal conductivity $\langle k\rangle_{yy}$ with respect to porosity. The difference with the results of the unit-cell model notes that the heat transfer is significantly hindered by the pore-network randomness.

4.2 Lateral Effective Conductivity

Due to the anisotropic pore morphology, the effective conductivity is not isotropic and a preferential conduction occurs along the y direction, shown in Fig. 1. The predicted variation of the lateral effective conductivity $\langle k\rangle_{xx}$ with respect to porosity is shown in Fig. 10. Here the ratio $\langle k\rangle_{xx}/\langle k\rangle_{yy}$ is also used to emphasize the anisotropy. There are no available experimental data for comparison. The overall trend in the porosity dependency is similar to that of $\langle k\rangle_{yy}$. The pore branches completely break the solid-phase connectivity and the resulting serial arrangement of phases leads to a very low thermal conductivity. Bakker (1997) ascertained that two dimensional conductivity is a lower limit of three dimensional conductivity due to the extra degree of freedom of heat flow in three dimension.

4.3 Size effect

There exist regimes of size where the macroscopic laws are no longer applicable (Majumdar, 1993; Tien and Chen, 1994; Chen, 1998). Recent experiments show that phonon scattering at the interface of small, dissimilar materials is considerable enough to reduce the heat transfer rate (Capinski and Maris, 1996; Yu et al., 1995; Lee and Cahill, 1997). According to Flick et al. (1992), the size effect on heat conduction becomes important when $\langle d\rangle<7\lambda_p$. For porous silicon at near room-temperature, the mean-free path can be estimated according to Eq. (2). The thermal conductivity ($k_s=149$ W/m-K) and the volumetric heat capacity ($\rho c_{v,p}=1.659\times10^6$ J/m^3-K) of the bulk silicon are used (Kaviany, 1998). A special average of the transverse and longitudinal phonon velocity, $u_p^{-1}=\frac{1}{3}(2u_{p,T}^{-1}+u_{p,L}^{-1})^{-1}=6.53\times10^3$ m/s is used for the average phonon velocity (Holland, 1963). This gives the bulk phonon mean-free path $\lambda_{p,0}\sim40$ nm, which is larger than the pore size of porous silicon considered here. This implies that the small pore size of porous silicon has an effect on the observed low thermal conductivity.

For accurate treatment of the size effect, the Boltzmann transport equation should be solved,

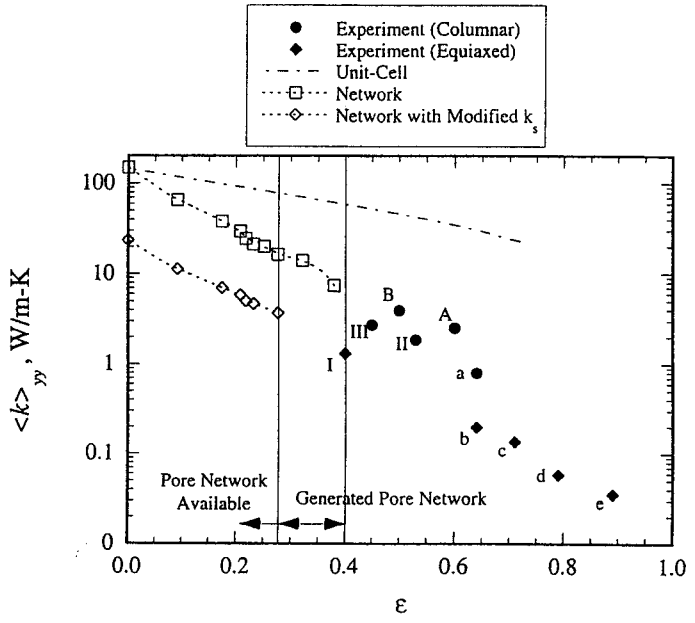

Fig. 11 Comparison of the predicted effective thermal conductivity of porous silicon $\langle k \rangle_{yy}$, with the availble experiments.

but this is not attempted here. Majumdar (1993) has derived an equation of phonon radiative transfer from the Boltzmann transport equation and suggests a modified mean-free path expressed as

$$\lambda_p = \frac{\lambda_{p,0}}{1+\frac{4}{3}\frac{\lambda_{p,0}}{\langle d \rangle}} \tag{5}$$

which may be used to determine k_s in Eq. (2). Also shown in Fig. 9 is the result using Eq. (5) with $d=10$ nm. This gives $\lambda_p=0.158\ \lambda_{p,0}$, which gives a solid conductivity $k_s=23.5$ W/m-K. This pore size, $d=10$ nm is consistent with those of experimental samples A, B and a in Figure 11. A closer agreement with the experiment is found.

A more simple prediction is possible based on the assumption that thermal conductivity is proportional to the mean distance, which the heat travels without any disturbance. This is similar to kinetic theory. The difference is that in kinetic theory, the mean-free path is by phonon but here the mean-solid phase distance. Since the thermal conductivity ratio of porous silicon is very large (5.56×10^3), most of the heat is transferred through the solid phase and the pore plays a role similar to that of the scattering source in kinetic theory. This similarity gives a good prediction as shown in Fig. 9 (bold line) by simply multiplying a constant to the mean-solid phase distance of each pore structure.

4.4 Comparison with experiments

The available experimental results are too few and inconsistent. They also lack sufficient geometrical information for a direct comparison with the predictions. Drost et al.(1995) used a dynamic conductivity measurement technique based on the thermal waves traveling in the specimen. However, as mentioned by Benedetto et al.(1997), the measurement technique by Drost et al.(1995) is rather complicated and cannot be used for different sample types. Also, the undesirable effect of SiC layers in the dynamic conductivity measurement, should be removed. Benedetto et al.(1997) measured $\langle k \rangle_{yy}$ for porous-silicon layers using a photoacoustic technique and Gesele et al.(1997) used the 3-ω technique. The measurements are summarized in Table 2. Among the parameters, the porosity, the morphology, and the pore size are used in the prediction. The pore sizes reported by Drost et al.(1995), and Gesele et al.(1997), are well documented. However the pore sizes in the

Table 2 The doping and etching parameters with the experimental results for various porous silicon samples.

Sample	A	B	C	D	I	II	III	a	b	c	d	e
resistivity, ρ_e Ohm-cm	0.01	0.01	10	10	38.0 -52.0	1-2	0.010 -0.018	0.01	0.02			
HF concentration, %	20	12	12	12	-	-	-	48				
current density, mA/cm^2	15	15	86	86	30	10	50	-				
etching time, s	1800	1800	720	3000	420	900	240	-				
illumination applied	-	-	none	none	none	halogen	none	-				
porosity, ε	0.60	0.50	0.40	0.40	0.40	0.53	0.45	0.64	0.64	0.71	0.79	0.89
layer thickness, δ, μm	23	10	75	175	10	10	10	21	31	31	31	35
silicon wafer type	p^+	p^+	n^-	n^-	p^-	n	p^+	p^+	p			
morphology	columnar				equiaxed	columnar			equiaxed			
pore size, d, nm	>12	~ 12	-	~ 500 /~ 200	~ 3	≥ 100	~ 100	9.0 ± 3.0	1.7 ± 0.5	2.0 ± 0.3	2.7 ± 0.3	4.5 ± 0.6
$\langle k \rangle_{yy}$, W/m-K	2.5	3.9	31.2	10.4/ 31.2*	1.2/1.3**	1.75/1.85	80/2.7	0.79	0.196	0.135	0.058	0.035

A-D: Benedetto et al. (1997) I - III: Drost et al. (1995) a-e: Gessele et al. (1997)

* 2 layers. One layer of $\langle k \rangle_{yy}=10.4$ with pore diameter 500 nm and the other of $\langle k \rangle_{yy}=31.2$ with pore diameter 200 nm.

** The upper parts are for the specimen as prepared and the lower parts are for the oxidized specimen.

experiment by Benedetto et al.(1997), are not given and are assumed to be similar to those in the experiments by Beale et al.(1985).

The experimental results for $\langle k \rangle_{yy}$ are shown along with the various predictions in Fig. 11. Samples A, B, II, III, and 'a' have similar highly-branched, columnar pore structures as shown in Fig. 4, Sample III shows a large difference between the oxidized and fresh samples, and the high values are not in line with the other experimental results. Note that the n-type silicon sample with the light illumination (II), is very similar to the p-type silicon samples (A, B, III and a). The important difference is in its large pore size ($\langle d \rangle \sim 100$ nm) compared to the p-type samples ($\langle d \rangle \sim 10$ nm for A, B, and a). Sample C is also n-type, but light illumination is not applied. Smith and Collins (1992) report that the pore-like strait cylindrical channels are produced for this sample. Thus for sample C, the heat flow is not prohibited as much as the highly branched structures. This explains the large effective thermal conductivity of sample C. The results for sample III without oxidation are questionable because the measured thermal conductivity is near the value for the parallel arrangement of phases and the theoretical upper limit.

Samples I and b~e also have similar pore structures, i. e., equiaxed structures. Their thermal conductivities follow the same trend. However, they are lower than those of columnar structures, which are expected from the relatively smaller pore sizes of equiaxed structues.

With the random pore network, the predicted effective thermal conductivity using the Fourier treatment is shown in Fig. 11. As evident, overall agreement is acceptable but the predicted effective thermal conductivity is larger than the experiments. This may be due to the size effect (pore scattering). In a following paper, the low-dimensionality effect is directly included in a Boltzmann treatment of phonon transport.

5. Conclusion

Direct simulation of conduction through anisotropic porous silicon is made using the two-dimensional matrix structure from the diffusion-limited model. The effective conductivity tensor is highly anisotropic. It is shown that to a limited extent, the low-porosity structures can be extrapolated to higher porosity by manipulating the digital data. The matrix model predicts the relevant experimental results fairly well if extrapolations to slightly higher porosities are made. The low-dimensionality effect becomes important for small pore sizes and the modification of the solid conductivity, to account for the size effect, does appear to include this effect. Further low-dimensionality analysis, including a Boltzmann transport simulation, is needed for clarification. More convincing experimental results with documented pore geometry will be of great value.

Acknowledgments

The author is thankful to Professor Collins for the digital data from his simulations. He would like to express his appreciation to the Korea Science and Engineering Foundation for financial support.

References

Bakker, K., 1997, "Using the Finite Element Method to Compute the Influence of Complex Porosity and Inclusion Structures on the Thermal and Electrical Conductivity," *Int. J. Heat Mass Transfer*, Vol. 40, pp. 3503~3511.

Bauer, T. H., 1993, "A General Analytical Approach Toward the Thermal Conductivity of Porous Media," *Int. J. Heat Mass Transfer*, Vol. 36, pp. 4181~4191.

Beale, M. I. J., Benjamin, J. D., Uren, M. J., Chew, N. G. and Cullis, A. G., 1985, "An Experimental and Theoretical Study of the Formation and Microstructure of Porous Silicon," *Journal of Crystal Growth*, Vol. 73, pp. 622~636.

Benedetto, G., Boarino, L. and Spagnolo, R., 1997, "Evaluation of Thermal Conductivity of Porous Silicon Layers by a Photoacoustic Method," *Appl. Phys. A*, Vol. 64, pp. 155~159.

Canham, L. T., 1997, "Porous Semiconductors: A Tutorial Review," *Mat. Res. Soc. Symp. Proc.*, Vol. 452, pp. 29~42.

Capinski, W. S. and Maris, H. J., 1996, "Thermal Conductivity of GaAs/AlAs Superlattices," *Physica B*, Vol. 219&220, pp. 699~701.

Chen, G, 1998, "Thermal Conductivity and Ballistic-Phonon Transport in the Cross-Plane Direction of superlattices," *Physical Review B*, Vol. 57, pp. 14958~14973.

Drost, A., Steiner, P., Moser, H. and Lang, W., 1995, "Thermal Conductivity of Porous silicon," *Sensors and Materials*, Vol. 7, pp. 111~120.

Flik, M. I., Choi, B. I. and Goodson, K. E., 1992, "Heat Transfer Regimes in Microstructures," *ASME Journal of Heat Transfer*, Vol. 114, 666~674.

Gesele, G. Linsmeier, J., Drach, V. and Arens-Fischer, R., 1997, "Temperature-Dependent Thermal Conductivity of Porous Silicon," *J. Phys. D: Appl. Phys.*, Vol. 30, pp. 2911~2916.

Hoefner, M. L. and Fogler, H. S., 1988, "Pore Evolution and Channel Formation During Flow and Reaction in Porous Media," *AIChE Journal*, Vol. 34, pp. 45~54.

Holland, M. G., 1963, "Analysis of Lattice Thermal Conductivity," *Physical Review*, Vol. 132, pp. 2461~2471.

Kaviany, M., 1995, *Principles of Heat Transfer in Porous Media*, 2nd edn., Springer-Verlag, New York.

Kaviany, M., 1998, *Principles of Heat Transfer*, Course Pack, University of Michigan.

Kim, C. -J. and Ro, S. T., 1995, "A Block-Correction Aided Strongly Implicit Solver for the Five-Point formulation of elliptic differential equations," *Int. J. Heat Mass Transfer*, Vol. 38, pp. 999~1008.

Lee, S. L. and Yang, J. H., 1998, "Modelling of Effective Thermal Conductivity for a Non-homogeneous Anisotropic Medium," *Int. J. Heat Mass Transfer*, Vol. 41, pp. 931~937.

Lee, S. -M. and Cahill, D. G., 1997, "Thermal Conductivity of Si-Ge Superlattices," *Appl. Phys.*

Lett., Vol. 70, 2957~2959.

Majumdar, A. , 1993, "Microscale Heat Conduction in Dielectric Thin Films," *ASME Journal of Heat Transfer*, Vol. 115, pp. 7~16.

Nishioka, K., Murayama, T. and Ono, Y., 1996, "Estimation of Effective Thermal Diffusivity of Porous Solid Using Data for Image Processing," *ISIJ International*, Vol. 36, pp. 150~155.

Nozad, I., Carbonell, R. G. and Whitaker, S., 1985, "Heat Conduction in Multi-Phase System I: Theory and Experiments for Two-Phase Systems," *Chem. Engng Sci.*, Vol. 40, pp. 843~855.

Patankar, S. V., 1980. *Numerical Heat Transfer and Fluid Flow*, Hemisphere, Washington, DC.

Schneider, P. J., 1985, Conduction. In *Handbook of Heat Transfer Fundamentals*, 2nd edn., ed. Rohsenow, W. M., Hartnett, J. P. and Ganic, E. N., McGraw-Hill Book Company, New York, Chapter 4.

Smith, R. L., Chuang, S. -F. and Collins, S. D., 1988, "A Theoretical Model of the Formation Morphologies of Porous," *J. Electron. Mater*, Vol. 17, pp. 533~541.

Smith, R. L. and Collins, S. D., 1989, "Generalized Model for the Diffusion-Limited Aggregation and Efen Models of Cluster Growth," *Physical Review A*, Vol. 39, pp. 5409~5413.

Smith, R. L. and Collins, S. D., 1992, "Porous Silicon Formation Mechanisms," *J. Appl. Phys.*, Vol. 71, pp. R1~R22.

Tien, C. -L. and Chen, G., 1994, "Challenges in Microscale Conductive and Radiative Heat Transfer," *Journal of Heat Transfer*, Vol. 116, pp. 799~807.

Touloukian, Y. S., Powell, R. W., Ho, C. Y. and Klemens, P. G., 1970, *Thermophysical Properties of Matter*, IFI/PLENUM, New York -Washington.

Tsao, S. S., Guilinger, T. R. and Kelly, M. J., 1991, "Porous silicon formation in $n^-/n^+/n^-$ Doped structures," *J. Electrochem. Soc.*, Vol. 138, pp. 1739~1743.

Yu, X. Y., Chen, G., Verma, A. and Smith, J. S., 1995, "Temperature Dependence of Thermophysical Properties of GaAs/AlAs Periodic Structure," *Appl. Phys. Lett.*, Vol. 67, pp. 3554 ~3556.

Ziman, J. M., 1960, *Electron and Phonons*, Oxford University Press, Oxford.